Journal of Physics: Conference Series **2894** (2024) 012020 doi:10.1088/1742-6596/2894/1/012020

All-Optical Vacuum Birefringence with PW-Class Lasers: Case Study for the ELI-NP Parameters

Stefan Ataman, Yoshihide Nakamiya, Mădălin Roşu, Liviu Neagu, Ovidiu Teşileanu

Extreme Light Infrastructure - Nuclear Physics (ELI-NP),
"Horia Hulubei" National R&D Institute for Physics and Nuclear Engineering (IFIN-HH),
30 Reactorului Street, 077125 Bucharest-Măgurele, Romania

E-mail: stefan.ataman@eli-np.ro

Abstract. In this paper we discuss the possibility of vacuum birefringence detection via all-optical, interferometric schemes. ELI-NP's laser parameters are employed, hence the pump is considered to be a 10 PW laser while the probe is a much weaker one ($\sim$ GW to TW). We assess two collision geometries and deduce the ideal probe pulse duration. We then go on and discuss the output signal of a balanced Mach-Zehnder interferometer and also propose two technically feasible experimental setups.

1. Introduction

Alongside with light-by-light (LBL) scattering [1, 2] and unassisted vacuum pair creation [3], vacuum birefringence (VB) [4, 5] is still an untested QED (quantum electrodynamics) prediction, in spite of the decades-long effort [6] to detect it. These still-to-be tested phenomena belong to what is usually called strong-field QED [7, 8].

First considered by Klein and Nigam [4], VB is usually discussed in terms of an effective theory [5]. This allows the description of a propagating probe beam in a stronger field, called pump [5, 7, 9]. The effective electromagnetic theory stemming from the Heisenberg-Euler (HE) Lagrangian [10] is usually approximated at its lowest orders [11] and it is a non-linear one. Other non-linear electrodynamics theories exist, the most prominent one being the one proposed by Born and Infeld (BI) [12]. Remarkably, while predicting LBL scattering, the BI theory predicts no VB.

VB measurement experiments are usually based on strong magnetic fields and optical cavities (*e. g.* PVLAS [6], BMV [13]). However, the last decade saw the emergence of a number of PW-class laser facilities [14], such as QST [15], GIST [16] or ELI-NP [17, 18]. Thus, unprecedented electromagnetic fields reaching intensities of 10^{23} W/cm^2 became available. This availability facilitated the appearance of the second category of vacuum birefringence measurement proposals, namely the ones based on a PW-class laser pump. Experiments employing a γ-beam probe have been proposed (King & Heinzl [19], Bragin *et al.* [20], Nakamiya & Homma [21]). The observable for this experiments is the polarization flip [22] of a high energy probe photon in the intense laser field. They benefit from the high flip probability ($\sim$ 30 % [21]), however accurate polarimetric detection of GeV gamma rays is an ongoing challenge [21]. Another large number of experimental proposals employ an X-ray probe and a PW-class beam

[23, 24, 25, 26, 27]. This category of experiments is particularly appealing due to the availability of high-precision X-ray polarimetry.

Early proposals for fully all-optical PW-laser based VB measurement were due to Luiten & Petersen [28], where a cavity-based polarimetric scheme was advocated. Another category of all-optical vacuum bireringence measurement schemes is one based on optical phenomena of a disturbed quantum vacuum and where we can include vacuum diffraction [29], reflection [30] and interference [31]. A Mach-Zehnder based proposal was introduced in reference [32] and subsequently refined [33]. Based on this proposal, in this work we elaborate on the VB signal feasibility for a MZI-based scheme by employing ELI-NP's laser parameters.

This paper is structured as follows. In Section 2 we introduce the Lagrangian describing the theory and deduce the VB for the laser pump-probe geometry we consider. In Section 3 we estimate the expected QED-induced phase shift and find the needed conditions in order to be detectable by interferometry. A detailed discussion of the MZI VB detection scheme is given in Section 4. Finally, conclusions are drawn in Section 5.

2. From QED to vacuum birefringence, via the Heisenberg-Euler Lagrangian

2.1. From nonlinear Lagrangians to vacuum phenomena

Let us consider the non-linear Lagrangian [34]

$$\mathcal{L}_{NL} = \frac{\mathcal{F}}{2} + c_1\mathcal{F}^2 + c_2\mathcal{G}^2 \tag{1}$$

where the two invariants of the electromagnetic field are $\mathcal{F} = \epsilon_0\left(E^2 - c^2B^2\right)$ and $\mathcal{G} = \sqrt{\varepsilon_0/\mu_0}\boldsymbol{E}\cdot\boldsymbol{B}$. If one assumes $c_1 = 4c_2$, the Lagrangian from equation (1) represents the lowest order expansion of the Born-Infeld (BI) [12] theory. If we take the two coefficients to be $c_1 = \Lambda_{EK}$ and $c_2 = 7\Lambda_{EK}$, then equation (1) represents the lowest order nonlinear expansion of the Heisenberg-Euler (HE) Lagrangian [10, 35], where we have the constant[1] $\Lambda_{EK} = \frac{\alpha}{90\pi\varepsilon_0 E_S^2} \approx 1.65\times10^{-30}\ \left[\mathrm{m}^3/\mathrm{J}\right]$. In the following we will focus on the VB predicted by the HE Lagrangian.

2.2. Vacuum birefringence for counter-propagating pump-probe laser beams

A linearly polarized probe field $\boldsymbol{E}_p = E_p\hat{\boldsymbol{x}}$ ($\boldsymbol{B}_p = -B_p\hat{\boldsymbol{y}}$), with $E_p, B_p \geq 0$ propagating along the negative z-axis ($\boldsymbol{k}_p = -|\boldsymbol{k}_p|\hat{\boldsymbol{z}}$) and in perpendicular electric and magnetic pump fields will see the refraction indices [34, 36]

$$\begin{cases} n_\perp - 1 = 7\varepsilon_0\Lambda_{EK}c^2B_0^2 + 7\varepsilon_0\Lambda_{EK}E_0^2 + 14\varepsilon_0\Lambda_{EK}cE_0B_0 \\ n_\parallel - 1 = 4\varepsilon_0\Lambda_{EK}c^2B_0^2 + 4\varepsilon_0\Lambda_{EK}E_0^2 + 8\varepsilon_0\Lambda_{EK}cE_0B_0 \end{cases} \tag{2}$$

where in the "$\perp$" case we have $\boldsymbol{E}_0 = -E_0\hat{y}$ and $\boldsymbol{B}_0 = B_0\hat{x}$ while in the "$\parallel$" one $\boldsymbol{E}_0 = E_0\hat{x}$ and $\boldsymbol{B}_0 = B_0\hat{y}$ and $E_0, B_0 \geq 0$. The B_0^2 terms represents the Cotton-Mouton (CM) effect, the E_0^2 ones denote the so-called Kerr effect while the last ones the magneto-electric effect. In this work we assume the pump field to be a counter-propagating (or nearly counter-propagating, to be detailed later) laser field ($E_L = cB_L$) having $\boldsymbol{E}_L = E_L\hat{\boldsymbol{x}}$ in the "$\parallel$" scenario and $\boldsymbol{E}_L = -E_L\hat{\boldsymbol{y}}$, in the "$\perp$" one (see Fig. 1). For simplicity, both the pump and the probe are assumed to be

[1] In the previous equations ε_0 (μ_0) represents the electric permittivity (magnetic permeability) of the vacuum, $c = 1/\sqrt{\varepsilon_0\mu_0}$ is the speed of light in vacuum, e (m) denotes the charge (mass) of the electron, h ($\hbar = h/2\pi$) is the (reduced) Planck constant and the QED fine-structure constant is defined, as usual by $\alpha = e^2/4\pi\varepsilon_0\hbar c \approx 1/137$. The Sauter-Schwinger critical field is given by $E_S = m^2c^3/e\hbar$.

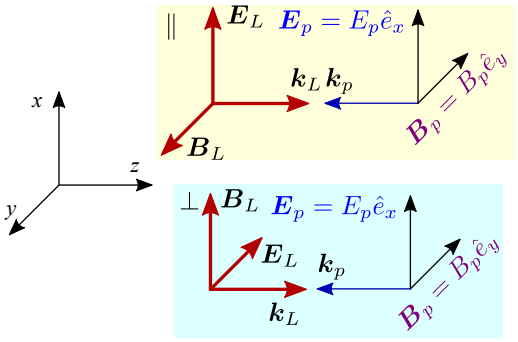

Figure 1. The pump-probe collision geometry. Both (pump and probe) are assume to be linearly polarized monochromatic laser beams.

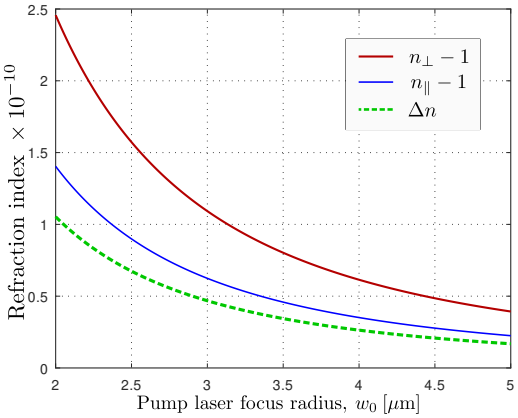

Figure 2. Expected refraction indices versus the focused radius for the ELI-NP 10 PW laser. For parameters, see Tab. 1.

Table 1. Parameters of the considered lasers.

The considered laser	Rated power P_L [PW]	Pulse duration τ_L [fs]	Pulse energy $\mathcal{E}_L$ [J]
ELI-NP 10 PW	10 PW	25	250
ELI-BL L4 Aton	10 PW	150	1500

nearly monochromatic. The probe beam counter-propagating in strong laser field will see the refraction indices [23, 33, 37]

$$\begin{cases} n_\perp = 1 + 28\varepsilon_0\Lambda_{EK}E_L^2 = 1 + 56\frac{\Lambda_{EK}}{c}I_L \\ n_\parallel = 1 + 16\varepsilon_0\Lambda_{EK}E_L^2 = 1 + 32\frac{\Lambda_{EK}}{c}I_L \end{cases} \tag{3}$$

implying a VB

$$\Delta n = n_\perp - n_\parallel = 24\frac{\Lambda_{EK}}{c}I_L \approx 2.6\times 10^{-33}\times I_L\left[\frac{\mathrm{W}}{\mathrm{cm}^2}\right] \tag{4}$$

where the intensity of the pump beam is[2] $I_L = \varepsilon_0 c E_L^2/2$.

For ELI-NP's 10 PW laser (see Tab. 1) we have an estimated $\Delta n \sim 10^{-10}$ *i. e.* a refraction index 13 orders of magnitude above the magnetic-only scenarios [6]. Noteworthy, ELI-Beamlines' Aton laser is expected to yield the same VB signal. Further assuming the pump to be a Gaussian beam having the focused waist radius w_0 and a duration τ_L, we have a maximum focused intensity

$$I_{L,max} = \frac{\mathcal{E}_L}{\pi\tau_L w_0^2}. \tag{5}$$

where $\mathcal{E}_L$ denotes the pump pulse energy. Combining the previous result with equations (3) and (4) allows one to express both $n_\perp/n_\parallel$ and Δn in respect with the pump waist radius. The results are plotted in in Fig. 2.

[2] We assume the pump field to be monochromatic, the intensity is thus connected to its "effective" value $E_L/\sqrt{2}$, hence the factor of 2 taken in our definition of I_L.

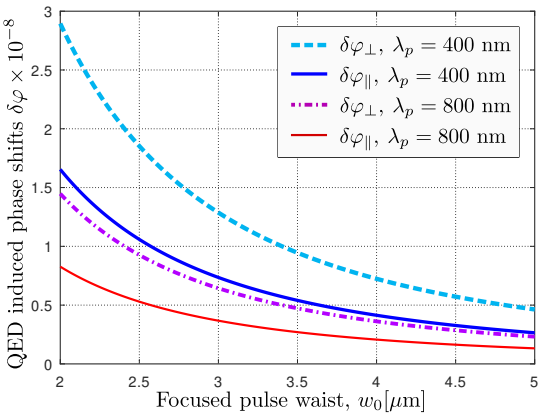

Figure 3. Expected QED-induced phase shifts for ELI-NP's 10 PW laser. Two probe wavelengths are considered, $\lambda_p = 800$ nm and its SHG, $\lambda_p = 400$.

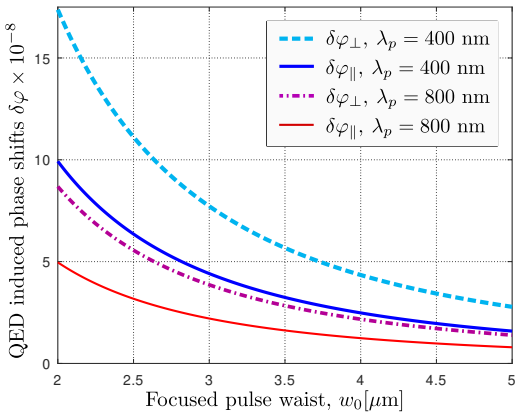

Figure 4. Expected QED-induced phase shifts for ELI-Beamlines' 10 PW Aton laser. Two probe wavelengths are considered, $\lambda_p = 800$ nm and $\lambda_p = 400$.

3. VB signal measurement via classical and non-classical interferometry

3.1. From intense-field QED to interferometry

We now focus on the probe beam, assumed to have a wavelength λ_p, hence an angular frequency $\omega_p = 2\pi c/\lambda_p$. While counter-propagating (with $\perp$ and, respectively, $\parallel$ polarization wrt the pump laser) through a pump-disturbed vacuum (over a length $z_{int} = c\tau_L$) it accumulates the phases

$$\left\{ \begin{array}{c} \varphi_\perp \\ \varphi_\parallel \end{array} \right\} = \frac{\omega_p z_{int}}{c} \times \left\{ \begin{array}{c} n_\perp \\ n_\parallel \end{array} \right\} \tag{6}$$

and compared to a "true" vacuum propagation we have the phase shifts

$$\left\{ \begin{array}{c} \delta\varphi_\perp \\ \delta\varphi_\parallel \end{array} \right\} = 2\pi\Lambda_{EK} \times \left\{ \begin{array}{c} 56 \\ 32 \end{array} \right\} \times \frac{\tau_L I_L}{\lambda_p} = 16\Lambda_{EK} \times \left\{ \begin{array}{c} 7 \\ 4 \end{array} \right\} \times \frac{\mathcal{E}_L}{\lambda_p w_0^2}. \tag{7}$$

Plugging in ELI-NP's 10 PW laser parameters leads us to the expected order of magnitude for our signal,

$$\delta\varphi_{qed} \approx \{\delta\varphi_\parallel, \delta\varphi_\perp\} \sim 10^{-8} \text{ rad}. \tag{8}$$

Employing equation (7), we can plot the expected VB-induced phase shifts in respect with the focused waist radius of the pump beam for ELI-NP's 10 PW laser (see Fig. 3) as well as ELI-Beamlines' upcoming Aton laser (see Fig. 4). We do this for both the "baseband" probe wavelength ($\lambda_p = 800$ nm) (red and magenta curves) and well as its SHG (second harmonic generation), $\lambda_p = 400$ (blue and light blue curves).

3.2. Classical and non-classical phase shift interferometry

In the case of interferometric phase measurement, one of the most important parameters is the average number of input photons, $\bar{N}$. Assuming our probe beam to have a pulse duration τ_p (to be defined later), we have the relation

$$\bar{N} = \frac{\mathcal{E}_p}{\hbar\omega_p} = \frac{P_p\tau_p}{\hbar\omega_p} \tag{9}$$

where P_p ($\mathcal{E}_p$) denotes the probe power (energy). For shot-noise limited (SNL) interferometry [38], the phase sensitivity is lower bounded by $\Delta\varphi_{SNL} = 1/\sqrt{\bar{N}}$. In order to detect a VB signal, we need to impose

$$\frac{1}{\sqrt{\bar{N}}} = \Delta\varphi_{SNL} \leq \delta\varphi_{qed} \tag{10}$$

leading us to the required minimum number of probe photons $\bar{N} \geq 1/(\delta\varphi_{qed})^2 \sim 10^{16}$. This limit applies, for example, if one uses a laser probe beam (*i. e.* classical input or *coherent light* in quantum optics (QO) parlance). From equation (9) we obtain the minimum shot-noise-limited probe power,

$$P_p \geq \frac{\hbar\omega_p}{(\delta\varphi_{qed})^2\tau_p}. \tag{11}$$

For ELI-NP's 10 PW pump laser we obtain the range of minimum probe powers $P_p \sim [0.01, 5]$ TW for $w_0 \leq 5\,\mu$m in order to reach the target phase sensitivity. We will return to this subject shortly. Quantum metrology, however, can provide a much more convenient scaling via the so-called Heisenberg limit (HL), $\Delta\varphi_{HL} = 1/\bar{N}$ [38, 39]. We need to impose this time

$$\frac{1}{\bar{N}} = \Delta\varphi_{HL} \leq \delta\varphi_{qed} \tag{12}$$

and this constraint leads us to a minimum of $\bar{N} \geq 1/\delta\varphi_{QED} \sim 10^8$ probe photons and $P_p \geq \frac{\hbar\omega_p}{\delta\varphi_{QED}\tau_p}$. While theoretically possible, this limit is completely out of reach given today's technology. In order to emphasize this, we can consider two quantum states of light known to be able to reach the HL in an interferometric scheme. Consider first the so-called NOON states [40]. After decades of evolution, the current record is still below $\bar{N} \sim 10^2$, thus a mere 6 orders of magnitude below the requirements for this experiment. A more realistic state would be the popular coherent plus squeezed vacuum input [41]. However, for a HL scaling we need equal number of coherent and squeezed photons, in the order to $\sim 0.5 \times 10^8$. While for the former there is no technical problem, the latter would imply a squeezing factor $r = 9.5$, which is totally unrealistic with today's technology (current record $r = 1.15$ [42]). To these problems one has to add losses in a realistic scheme, their effect further degrading the quantum advantage [43].

However, one does not have to chase the elusive HL, achieving sub-SNL phase sensitivity being sometimes sufficient in order to reach the goal, as eloquently proved by the LIGO and Virgo collaborations [44]. For example, by employing a coherent plus squeezed vacuum input state in the realistic high-coherent regime ($|\alpha|^2 \gg \sinh^2 r$) results in the phase sensitivity

$$\Delta\varphi = \frac{e^{-r}}{\sqrt{|\alpha|^2}} \approx \frac{e^{-r}}{\sqrt{\bar{N}}} \tag{13}$$

and for current squeezing factors ($r \leq 2$) we have $\Delta\varphi \approx 0.1/\sqrt{\bar{N}}$. Application of this input state to the VB interferometric measurement is discussed in references [32, 33].

3.3. Two collision geometries

We now define the ideal probe pulse duration (τ_p), assumed to be adjustable. The actual factor determining it is the exact collision geometry. Starting with the "at an angle" geometry (see Fig. 5), the relevant probe duration is

$$\tau_p \approx \tau_L \tag{14}$$

because in this scenario meaningful pump-probe overlap happens only over a distance $z_{int} = c\tau_L$. For a fully counter-propagating geometry (see Fig. 6), we have an ideal pulse duration (see also the discussion in reference [33])

$$\tau_p \approx \frac{b}{c} = \frac{2z_R}{c} \tag{15}$$

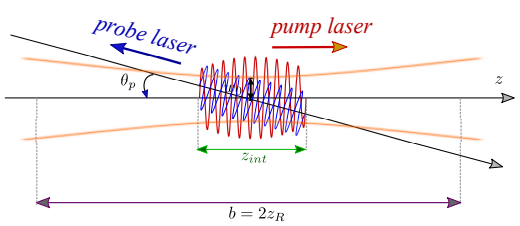

Figure 5. "At an angle" pump-probe collision geometry. Details are given in the main text.

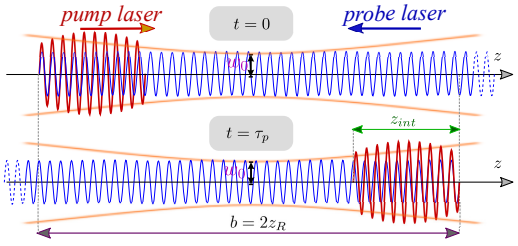

Figure 6. Head-on pump-probe collision geometry. Details are given in the main text.

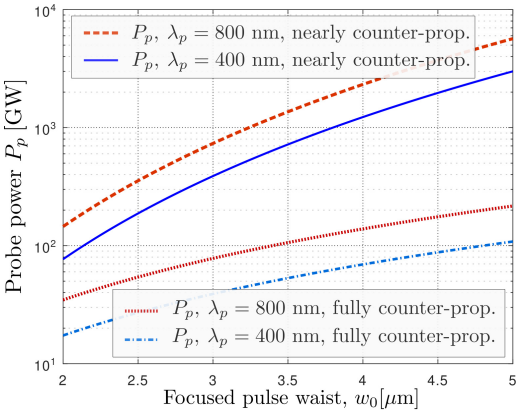

Figure 7. The minimum required probe power versus the focused waist radius w_0 for ELI-NP's 10 PW laser.

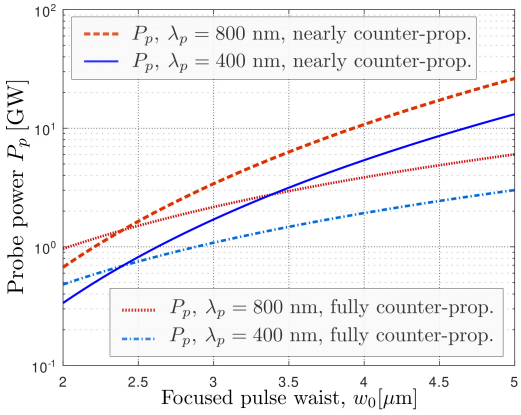

Figure 8. The minimum required probe power versus the focused waist radius w_0 for ELI Beamlines' 10 PW laser.

where the depth of focus ($b = 2z_R$) and the Rayleigh length $z_R = \pi w_0^2/\lambda_L$ are defined as usual. For ELI-NP's laser parameters and assuming a depth of focus in the range $w_0 \in [2, 5]\,\mu$m we get a range of ideal probe pulse durations $\tau_p \in [100, 700]$ fs.

We can now plot the minimum needed probe power versus the pump focus waist radius both for ELI-NP's 10 PW laser (see Fig. 7) and ELI-Beamlines' Aton 10 PW laser (see Fig. 8). We consider both "at an angle" and fully counter-propagating collision geometries as well as two probe wavelength, namely $\lambda_p = 800$ nm (red curves) and its SHG (second harmonic generation) $\lambda_p = 400$ (blue and light blue curves).

Since ELI-NP's pump pulse is rather short, the ideal probe duration from equation (15) is $\tau_p \gg \tau_L$, hence there is a noticeable difference between the "at an angle" and fully counter-propagating collision scenarios. This assertion, however is no longer true for ELI-Beamlines's Aton laser (see Fig. 8). Indeed, plugging $\tau_L = 150$ fs into equation (15), for $w_0 \leq 5\,\mu$m results in $\tau_L \sim \tau_p$, it thus becomes irrelevant what collision geometry one chooses in this case.

4. Detailed discussion of a Mach-Zehnder interferometer-based proposal

A Mach-Zehnder-based all-optical VB experiment was proposed in reference [32]. The schematic is depicted in Fig. 9. A counter-propagating laser creates a vacuum-disturbed region (gray blob) where the counter-propagating probe beam will experience an extra phase shift (compared to the upper arm), $\delta\varphi_{qed}$. Throughout this work we consider both beam splitters balanced (50/50) and ignore internal as well as photo-detection losses.

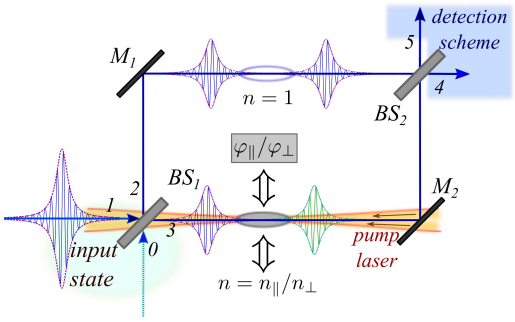

Figure 9. The Mach-Zehnder-based all-optical VB detection scheme. The counter-propagating pump laser disturbs the vacuum around its focus (gray blob), hence the probe beam experiences a slower propagation in the lower arm, compared to the upper one.

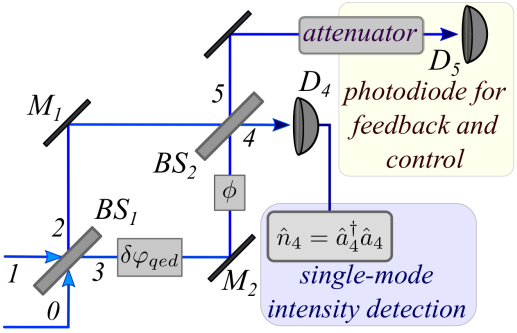

Figure 10. QO view of the interferometer with the single mode intensity detection scheme (modelled via the operator $\hat{n}_4$). The QED-induced phase shift $\delta\varphi_{qed}$ is complemented by the user-introduced phase shift ϕ whose role is to bring the MZI to its working point.

4.1. MZI phase sensitivity with a single coherent input

We consider the interferometric scheme fed by a coherent input, we can thus write the input state as [45]

$$|\psi_{in}\rangle = |\alpha_1 0_0\rangle \tag{16}$$

and the average number of photons for our input state is given by $\bar{N} = |\alpha|^2$ [45]. We split the internal phase shift into two components, the tiny QED-induced phase shift $\delta\varphi_{qed}$ and the experimentally controllable ϕ, so that $\varphi = \delta\varphi_{qed} + \phi$ (see Fig. 10). As we will discuss shortly, by adjusting ϕ to ϕ_{opt} we can put the MZI in its optimum working point (*i. e.* "sweet spot"). The phase sensitivity of an MZI with classical input state has been discussed at length in the literature [43, 45, 46, 47]. The optimum phase sensitivity one can expect is given by the so-called quantum Cramér-Rao bound[3] (QCRB) and for our setup it found to be [48]

$$\Delta\varphi_{QCRB} = \frac{1}{\sqrt{\bar{N}}} \tag{17}$$

and one recognizes here the SNL. Given the input state we consider, a suitable detection scheme is the so-called direct detection or single-mode intensity detection[4]. One finds the phase sensitivity

$$\Delta\varphi_{sg} = \frac{1}{\sqrt{\bar{N}}\left|\sin\frac{\varphi}{2}\right|} \tag{18}$$

with the optimum working point being obviously $\phi_{opt} = \pi$. Ne note that and by imposing ϕ_{opt} (recall that $\delta\varphi_{qed} \ll 1$) into equation (18) we reach the QCRB (17), our setup is thus *optimal*.

Since our detection is modelled by the photon number operator in output port 4 (denoted $\hat{n}_4$), by employing standard QO methods (see *e. g.* [43, 46, 47, 49]), we get the average number of photons at output port 4,

$$\langle\hat{n}_4\rangle = \cos^2\frac{\varphi}{2}\bar{N} \tag{19}$$

[3] Equation (17) should actually read $\Delta\varphi_{QCRB} = \frac{1}{\sqrt{\mathcal{N}\bar{N}}}$ where $\mathcal{N}$ is the number of repeated measurements [48]. However, for simplicity, we consider $\mathcal{N} = 1$ in this work.

[4] For a more detailed discussion about detection schemes in QO, the reader can consult references [43, 47, 49].

and the variance of the same operator yields $\Delta^2\hat{n}_4 = \cos^2\frac{\varphi}{2}\bar{N}$. The working point is $\phi_{opt} = \pi$ and the QED induced phase shift obeys $|\delta\varphi_{qed}| \ll |\varphi|$. One thus finds from equation (19) an average number of photons in the output port 4 near the optimum working point given by $\langle\hat{n}_4\rangle = (1 - \cos\delta\varphi_{qed})\,\bar{N}/2$ and applying a Taylor series[5] development we have

$$\langle\hat{n}_4\rangle = \frac{1}{4}(\delta\varphi_{qed})^2\bar{N}. \tag{20}$$

Using the same arguments, we get a similar result for the variance, $\Delta^2\hat{n}_4 = \frac{1}{4}(\delta\varphi_{qed})^2\bar{N}$ and as a quick check, by applying the error propagation formula (see *e. g.* [43, 47]) we get

$$\Delta\tilde{\varphi} = \frac{\sqrt{\Delta^2\hat{n}_4}}{\left|\frac{\partial\langle\hat{n}_4\rangle}{\partial\varphi}\right|} = \frac{1}{\sqrt{\bar{N}}} \tag{21}$$

and this is indeed the QCRB from equation (17), confirming once again that our detection scheme *is optimal* at its working point.

4.2. Realistic considerations with disturbances

In equation (20) we ignored the fact that in a realistic experiment small mis-alignments or vibrations (coming from the optical components, the optical table, vacuum systems etc.) will cause small offsets from the ideal working point. Let us denote ϕ_d these unwanted signals, so that we can write equation (19) as

$$\langle\hat{n}_4\rangle = \frac{1}{4}\left(\delta\varphi_{qed} + \phi_d\right)^2\bar{N} \approx \frac{1}{2}\phi_d\delta\varphi_{qed}\bar{N} + \frac{1}{4}\phi_d^2\bar{N} \tag{22}$$

and in the last step we ignored the $(\delta\varphi_{qed})^2$ term. Two scenarios open here: i) we have $\phi_d \gtrsim \delta\varphi_{qed}$ and ii) $\phi_d \gg \delta\varphi_{qed}$. In the scenario i), the output signal can be approximated to

$$\langle\hat{n}_4\rangle \approx \frac{1}{2}\delta\varphi_{qed}\phi_d\bar{N}. \tag{23}$$

We find a linear dependence on the desired signal *i. e.* $\langle\hat{n}_4\rangle \sim \delta\varphi_{qed}$, however in order to determine $\langle\hat{n}_4\rangle$ one needs to estimate ϕ_d for each PW laser shot, too. One can propose a setup that does not need to estimate ϕ_d, though. Indeed, for a probe beam linearly polarized at 45° relative to the pump beam, by employing a PBS separating the two output detectors (see Figs. 11 and 12) ones measures the ratio

$$\frac{\langle\hat{n}_{4,\perp}\rangle}{\langle\hat{n}_{4,\parallel}\rangle} \approx \frac{c_1}{4c_2} \tag{24}$$

and thus directly obtains the ratio of the coefficients from the Lagrangian (1). This contrasts will all proposed polarimetric schemes where one measures a phase shift $\delta \sim (4c_2 - c_1)$ [24].

In scenario ii), one needs to compensate ϕ_d. This scenario will be addressed in a future work.

[5] From equation (19) we have $\langle\hat{n}_4\rangle = (1 + \cos\varphi)\,\bar{N}/2 = (1 + \cos(\delta\varphi_{qed} + \pi))\,\bar{N}/2 = (1 - \cos\delta\varphi_{qed})\,\bar{N}/2$ and the Taylor series expansion for cosine $\cos(\delta\varphi_{qed}) = 1 - (\delta\varphi_{qed})^2/2! + (\delta\varphi_{qed})^4/4! + \ldots$. Since the expected $\delta\varphi_{qed} \sim 10^{-8}$ we have $(\delta\varphi_{qed})^4 \sim 10^{-32}$ and we totally disregard all terms beyond $(\delta\varphi_{qed})^2$. Due to the smallness of the neglected terms, we used the equal sign in equation (20) instead of the approximative one.

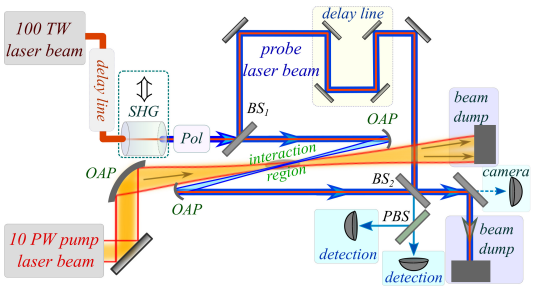

Figure 11. Mach-Zehnder based all-optical VB measurement setup with an "at an angle" collision geometry. The probe beam can be either used as is (red) or frequency double (blue).

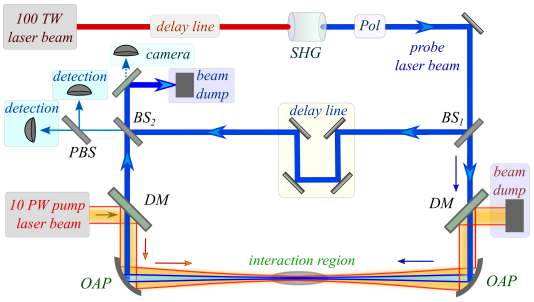

Figure 12. Mach-Zehnder based all-optical VB measurement setup with an fully counter-propagating pump-probe collision geometry. The probe beam is necessarily frequency doubled (blue).

4.3. Example implementations for the two collision geometries

Although several experimental setups can be proposed, we only illustrate two, in order to highlight the collisions geometries described in Section 3.3.

Let us start the discussion with the "at an angle" collision geometry depicted in Fig. 5. An example implementation is illustrated in Fig. 11. The probe beam polarization is set to 45° (by the block denoted "Pol"). This will result in the possibility to simultaneously detect via the polarizing beam splitter (PBS) the ratio of the Lagrangian's coefficient from equation (24). In this setup, one has the choice of using – or not – a SHG stage for the probe beam. The advantage of frequency doubling the probe beam results in a higher phase shift (see Fig. 7) and a much better filtering at the detection stage. The disadvantage lies in the conversion efficiency of the SHG stage.

A feature of employing high-intensity 10 PW pump lasers is the availability of a phase signal $\delta\varphi_{qed} \sim 10^{-8}$ rad. Another one is the possibility of collision geometry optimization for efficient interaction and via an adapted probe pulse duration (see Fig. 6). Thus, the longer interaction time with the pump pulse decreases the required peak probe power as done in the fully counter-propagating geometry (see Fig. 7). However, in this scenario, the SHG stage for the probe beam becomes compulsory. This brings us to the experimental setup from Fig. 12. The dichroic mirrors (DM) separate the two frequencies and the detection stage is similar to the one discussed previously. The disadvantages of this option originate mainly from the use of DMs in the MZI. Indeed, they can create non-trivial phase shifts while the probe light passes though dielectric coating.

Both setups are expected to suffer from the same parasitic signals including mechanical vibrations and the effect of residual gas in the focus area [33]. Both the estimation and the mitigation of these issues will be addressed at length in a future work.

5. Conclusion

In this paper we addressed the feasibility of an all-optical, vacuum birefringence experimental setup driven by a 10 PW pump laser. Although the expected phase shift is rather small ($\sim 10^{-8}$ rad), by using an interferometric scheme with a GW to TW probe laser, the QED-induced signal should be detectable at the shot-noise limit.

While many technical challenges still lie ahead, the theoretical feasibility of this setup motivates us to further explore all-optical, interferometric VB measurement schemes.

Acknowledgments
It is acknowledged that this research was supported from the Contract No. PN 23 21 01 05. It is also acknowledged that this work has been supported by the Extreme Light Infrastructure Nuclear Physics (ELI-NP) Phase II, a project co-financed by the Romanian Government and the European Union through the European Regional Development Fund and the Competitiveness Operational Programme (Grant No. 1/07.07.2016, COP, ID 1334).

References
[1] Halpern O 1933 *Phys. Rev.* **44** 855
[2] Costantini V, De Tollis B and Pistoni G 1971 *Nuov Cim A* **2** 733
[3] Breit G and Wheeler J A 1934 *Phys. Rev.* **46** 1087
[4] Klein J J and Nigam B P 1964 *Phys. Rev.* **135** B1279
[5] Bialynicka-Birula Z and Bialynicki-Birula I 1970 *Phys. Rev. D* **2** 2341
[6] Ejlli A *et al.* 2020 *Physics Reports* **871** 1
[7] Dittrich W and Gies H 2000 *Probing the Quantum Vacuum. Pertubative Effective Action Approach in Quantum Electrodynamics and its Application* (Springer)
[8] Fedotov A, Ilderton A, Karbstein F, King B, Seipt D, Taya H and Torgrimsson G 2023 *Phys. Rep.* **1010** 1
[9] Marklund M and Shukla P K 2006 *Rev. Mod. Phys.* **78** 591
[10] Heisenberg W and Euler H 1936 *Z. Physik* **98** 714
[11] Euler H and Kockel B 1935 *Naturwissenschaften* **23** 246
[12] Born M and Infeld 1934 *Proc. R. Soc. Lond. A* **144** 425
[13] Cadène A, Berceau P, Fouché M, Battesti R and Rizzo C 2014 *Eur. Phys. J. D* **68** 16
[14] Danson C N *et al.* 2019 *High Power Laser Science and Engineering* **7** e54
[15] Kiriyama H *et al.* 2020 *High Energy Density Physics* **36** 100771
[16] Sung J H *et al.* 2017 *Opt. Lett.* **42** 2058
[17] Galès S *et al.* 2018 *Reports on Progress in Physics* **81** 094301
[18] Radier C *et al.* 2022 *High Power Laser Science and Engineering* **10** e21
[19] King B and Heinzl T 2016 *High Power Laser Science and Engineering* **4** e5
[20] Bragin S, Meuren S, Keitel C H and Di Piazza A 2017 *Phys. Rev. Lett.* **119** 250403
[21] Nakamiya Y and Homma K 2017 *Phys. Rev. D* **96** 053002
[22] Dinu V, Heinzl T, Ilderton A, Marklund M and Torgrimsson G 2014 *Phys. Rev. D* **89** 125003
[23] Heinzl T, Liesfeld B, Amthor K U, Schwoerer H, Sauerbrey R and Wipf A 2006 *Opt. Comm.* **267** 318
[24] Schlenvoigt H P, Heinzl T, Schramm U, Cowan T E and Sauerbrey R 2016 *Physica Scripta* **91** 023010
[25] Shen B, Bu Z, Xu J, Xu T, Ji L, Li R and Xu Z 2018 *Plasma Physics and Controlled Fusion* **60** 044002
[26] Xu D, Shen B, Xu J and Liang Z 2020 *Nucl. Instrum. Methods. Phys. Res., Sect. A* **982** 164553
[27] Karbstein F, Ullmann D, Mosman E A and Zepf M 2022 *Phys. Rev. Lett.* **129** 061802
[28] Luiten A N and Petersen J C 2004 *Phys. Lett. A* **330** 429
[29] Tommasini D and Michinel H 2010 *Phys. Rev. A* **82** 011803
[30] Gies H, Karbstein F and Seegert N 2013 *New Journal of Physics* **15** 083002
[31] King B, Piazza A D and Keitel C H 2010 *Nature Photonics* **4** 92
[32] Ataman S 2018 *Phys. Rev. A* **97** 063811
[33] Ataman S 2023 *Journal of Physics: Conference Series* **2494** 012019
[34] Battesti R and Rizzo C 2013 *Reports on Progress in Physics* **76** 016401
[35] Schwinger J 1951 *Phys. Rev.* **82** 664
[36] Rikken G L J A and Rizzo C 2000 *Phys. Rev. A* **63** 012107
[37] Ahmadiniaz N *et al.* 2020 *Phys. Rev. D* **101** 116019
[38] Giovannetti V, Lloyd S and Maccone L 2006 *Phys. Rev. Lett.* **96** 010401
[39] Pezzè L, Hyllus P and Smerzi A 2015 *Phys. Rev. A* **91** 032103
[40] Afek I, Ambar O and Silberberg Y 2010 *Science* **328** 879
[41] Caves C M 1981 *Phys. Rev. D* **23** 1693–1708
[42] Vahlbruch H, Mehmet M, Danzmann K and Schnabel R 2016 *Phys. Rev. Lett.* **117** 110801
[43] Gard B T, You C, Mishra D *et al.* 2017 *EPJ Quantum Technology* **4** 4
[44] Tse M *et al.* 2019 *Phys. Rev. Lett.* **123** 231107
[45] Gerry C and Knight P 2005 *Introductory Quantum Optics* (Cambridge University Press)
[46] Pezzé L, Smerzi A, Khoury G, Hodelin J F and Bouwmeester D 2007 *Phys. Rev. Lett.* **99** 223602
[47] Ataman S, Preda A and Ionicioiu R 2018 *Phys. Rev. A* **98** 043856
[48] Paris M G A 2009 *International Journal of Quantum Information* **07** 125
[49] Ataman S 2019 *Phys. Rev. A* **100** 063821